JACS
JOURNAL OF THE AMERICAN CHEMICAL SOCIETY
Article
pubs.acs.org/JACS

Fluorinated Carbide-Derived Carbon: More Hydrophilic, Yet Apparently More Hydrophobic

Amir H. Farmahini,[†] David S. Sholl,[‡] and Suresh K. Bhatia*[,†]

[†]School of Chemical Engineering, The University of Queensland (UQ), Brisbane, Queensland 4072, Australia
[‡]School of Chemical and Biomolecular Engineering, Georgia Institute of Technology, Atlanta, Georgia 30332, United States

Supporting Information

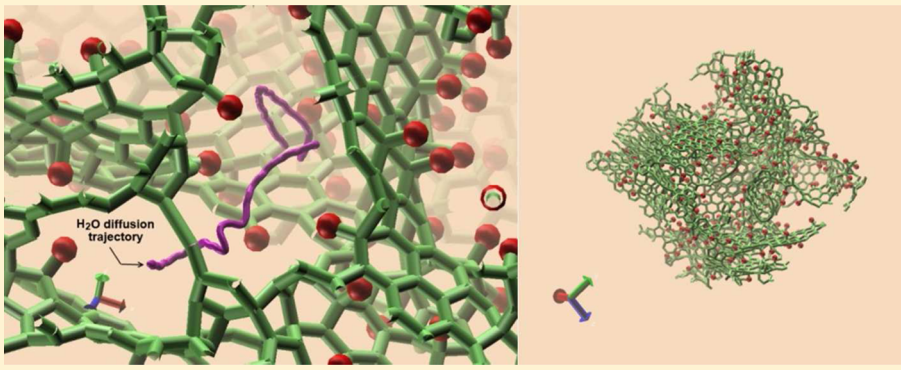

ABSTRACT: We explore the effect of fluorine doping on hydrophobicity of nanoporous silicon carbide-derived carbon (SiCDC), and investigate the underlying barriers for adsorption and diffusion of water vapor and CO_2 in the fluorinated and nonfluorinated structures. We develop atomistic models of fluorine-doped SiCDC at three different levels of fluorination, based on a hybrid reverse Monte Carlo constructed model of SiCDC, and develop a novel first-principles force field for the simulation of adsorption and transport of water and CO_2 in the fluorine-doped carbon materials. We demonstrate an apparent dual effect of fluorination, showing that while fluorination generates more hydrophilic carbon surfaces, they actually act as more hydrophobic structures due to enhanced energy barriers in the disordered network of microporous carbon. While an increase in adsorption energy and in water uptake is seen for fluorine-doped carbon, large internal free energy barriers as well as the results of MD simulations demonstrate that the increased adsorption is kinetically limited and not experimentally observable on practical time scales. We show that an increase in apparent hydrophobicity due to fluorination is mediated by larger free energy barriers arising from stronger binding of fluid molecules inside the pore network, as opposed to repulsion or steric hindrance to the diffusion of molecules through narrow pore entries. For carbon dioxide, adsorption enthalpies and activation energy barriers are both decreased on fluorination, indicating weakened solid−fluid binding energies in the fluorinated systems.

1. INTRODUCTION

The engineering of adsorbents to increase hydrophobicity is an area of much current interest, as moisture present in gas streams reduces the efficiency of processes for gas separation and storage. Fluorination of porous carbon has long been known to increase hydrophobicity,[1−5] and has found application not only in gas adsorption but also in proton exchange membrane (PEM) fuel cells and microfluidic devices.[6−9] Fluorine-doped graphite (poly(carbon monofluoride)) has been shown to be superhydrophobic,[10] based on the low sliding angles of water, while observations of high contact angle on fluorine-doped amorphous carbon films with diamond-like structure indicate these to be as hydrophobic as polytetrafluoroethylene (PTFE).[11] Nevertheless, despite such evidence, fundamental studies of the apparently water-repelling nature of fluorinated microporous carbon are scarce, and mechanistic understanding of the increase in hydrophobicity remains an open question.

Studies have shown that fluorination of activated carbon fiber (ACF) reduces N_2 adsorption, due to reduction in pore volume, surface area and pore size[12,13] and of the surface energy,[12] with the level of fluorination having an inverse relation with pore volume, surface area and average pore width of the sample.[13] Li et al.[14,15] reported significant reduction of N_2 and ethanol adsorption after fluorination of microporous ACF, which they attribute to reduction of micropore volume arising from pore blockage by C−F bonds. On the other hand, for water the observed decrease in adsorption was found to be much greater than that justified by the decrease in micropore volume. This they take to be an indication of increased hydrophobicity on fluorination and repulsive nature of the fluorine atoms,[14] since the basic microporous structure of the ACF was considered unaltered by fluorination while the

Received: February 1, 2015
Published: April 24, 2015

DOI: 10.1021/jacs.5b01105
J. Am. Chem. Soc. 2015, 137, 5969−5979

micropore wall structure adapted to the fluorinated state. Li et al.[15] hypothesized that water clusters cannot be formed on the fluorinated surface of F-ACF, while methanol and ethanol do adsorb in the form of molecular clusters due to attractive vdW interactions between their nonpolar functional groups and the hydrophobic surface of F-ACF. An interesting feature of their results is strong adsorption/desorption hysteresis for water, but its complete absence for methanol and ethanol. While the reasons for this were not discussed, the presence of significant energy barriers for water adsorption/desorption would appear likely. More recently, such hysteresis for water adsorption on virgin and mildly fluorinated activated carbon, and a decrease of water adsorption on fluorination has also been noted by Parmentier et al.[16] While they attribute the decrease of adsorption on fluorination to increased hydrophobicity, they also noted an increase in water content on the desorption branch for the fluorinated material for relative pressure below 0.5, an indication of increased hydrophilicity.

Thus, it is clear that while there exists experimental evidence for reduced water adsorption on fluorination, its interpretation in terms of the concept of hydrophobicity is tenuous. Fluorine-doped carbon forms a variety of complex covalently bonded substances whose chemical and structural properties are influenced by semi-ionic, ionic and van der Waals interactions.[17] Therefore, understanding the mechanism leading to reduction of water uptake, or increase of "hydrophobicity", requires fundamental knowledge of the adsorption process at molecular scales.

Here, we investigate the mechanisms underlying hydrophobicity of fluorinated microporous carbon to provide a clear description of this concept. The strong structure-dependence of adsorption necessitates access to a realistic representation of the microporous network of carbon atoms, which is nontrivial. To this end, we use a hybrid reverse Monte Carlo simulation-based atomistic model of silicon carbide-derived nanoporous carbon (SiCDC) for modeling fluorinated carbon samples. While this structural model has been extensively validated against adsorption data,[18−21] investigation of the effect of fluorination on adsorption, using this as a platform, is unique to this study. Here we design models of fluorinated silicon carbide-derived carbon (F-SiCDC) at three levels of fluorination, based on this virgin model, and investigate mechanisms underlying water adsorption in these materials.

We also report on development of a novel first-principles force field for the adsorption of water vapor and CO_2 in fluorinated microporous carbon structures. Our study demonstrates that while fluorination leads to more hydrophilic carbon surfaces, they actually act as more hydrophobic structures, due to enhanced energy barriers in the disordered microporous carbon network, revealing an apparent dual effect of fluorination.

2. COMPUTATIONAL DETAILS

Development of First-Principles Force Fields. We have developed a new first-principles force field for CO_2 and water vapor adsorption on fluorinated porous carbons. Considerable progress has been made in recent years on development of force fields for adsorption in porous materials, as reviewed by Fang et al.[22] We performed DFT calculations on a 22 × 22 Å sheet of fluorinated graphene containing 150 carbon and 17 fluorine atoms, having a circular defect at the center, of diameter ∼9 Å, on whose edge unsaturated carbon atoms are fluorinated. A 3 × 3 × 3 extended super cell of this structure, with interlayer distance equal to 20 Å, shown in Figure 1, was used for simulations. We used methods applied by Fang and co-workers to develop force fields for CO_2 adsorption in zeolites,[23−25] which have been validated for even smaller systems.

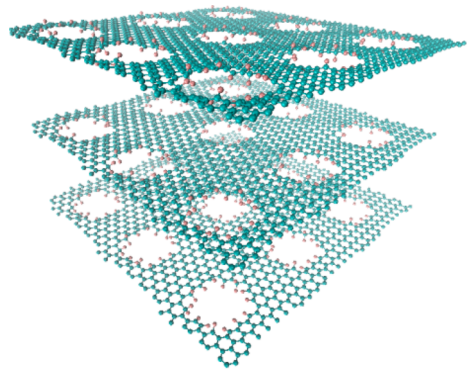

Figure 1. Fluorinated sheet of graphene with embedded defects in the form of pores.

Geometry optimization of the periodic system was performed using the dispersion-corrected DFT method of Grimme (DFT-D2)[26] implemented in VASP[27,28] following[23,24]

$$E_{\text{disp.}} = -s_6 \sum_{i=1}^{N-1} \sum_{j=i+1}^{N} \frac{C_6^{ij}}{r_{ij}^6} f_{\text{damp}}(r_{ij}) \quad (1)$$

where s_6 is a global scaling factor for each functional, N is the number of atoms, r_{ij} is the interatomic distance for atoms i and j, and finally C^{ij}_6 represents the dispersion coefficient. Electron−ion interactions were modeled using the projector augmented wave (PAW) formalism[29,30] with the Perdew−Burke−Ernzerhof (PBE) functional[31] chosen for the generalized gradient approximation (GGA). A plane wave basis set was employed with an energy cutoff of 400 eV for valence electrons. Reciprocal space was sampled at the Γ-point only. Geometry optimization was performed until forces on all atoms were smaller than 0.03 eV/Å.

Point charges on atoms in the fluorinated graphene were assigned using the density-derived electrostatic and chemical (DDEC) charges approach.[32−35] The DDEC method reproduces the electrostatic potential exactly outside the electron distribution by partitioning the electron and spin densities to compute net atomic charges and atomic spin moments.[32−35] The effect of polarization was investigated by calculating point charges of the fluorinated graphene in the presence of water molecules and comparing the results with charges for the isolated system. Polarization changed the total energy of the system by only 8.6%. Our results show that the mean absolute deviation of the charges in the polarized fluorinated graphene is 0.009e relative to the unpolarized graphene. Also, the mean absolute deviation of charges for polarized water molecules is equal to 0.03e relative to the SPC model used in our GCMC and MD simulations. Thus, polarization mainly affects the water molecules. We also note that the polarization effect is implicitly considered here, since we match the solid−fluid adsorption energy by fitting the parameters of the nonelectrostatic part of the force field, while retaining the electrostatic part in the SPC water model as discussed below. A similar approach has previously been adopted by Calero et al.,[36] in which effective Lennard−Jones interactions between the solid and weakly polarizable alkanes were used. A much more computationally intensive calculation would explicitly define a polarization term in the developed force field,[37] but was not attempted here.

Single point energy calculations (SPE) were performed for individual water and CO_2 molecules interacting with the fluorinated graphene using VASP. A large number of molecular configurations were randomly generated for adsorbate molecules in a simulation box containing the fluorinated graphene, to adequately sample the pore space. This includes both low and high-energy configurations of adsorbate molecules, so that the force field derived from our DFT data appropriately describes different energy states of the system for applications in grand canonical Monte Carlo (GCMC) and molecular

DOI: 10.1021/jacs.5b01105
J. Am. Chem. Soc. 2015, 137, 5969−5979

dynamics (MD) simulations. For SPE calculations, relaxation of the electronic degrees of freedom was terminated when variation of the total energy between two consecutive iterations was smaller than 0.0001 eV. The solid−fluid interaction energy of the system obtained from DFT calculations for all configurations was then fitted to the 12−6 LJ potential model augmented by electrostatic interactions:[23,24]

$$E_{ff}(r_{ij}) = E_{\mathrm{vdW}} + E_{\mathrm{Coul}} = s_{12}\frac{C_{12}^{ij}}{r_{ij}^{12}} - s_6\frac{C_6^{ij}}{r_{ij}^{6}} + \frac{q_i q_j}{\varepsilon_o r_{ij}} \quad (2)$$

Here, r_{ij} represents interatomic distances of ij pairs, C^{ij}_{12} and C^{ij}_{6} are repulsive and attractive coefficients respectively, q_i and q_j stand for atomic charges of atoms i and j, and ε_o is the permittivity of free space. s_{12} and s_6 are global scaling factors for force field fitting. In this equation, charges for water were taken from the SPC model[38] and for CO_2 from a model described by Nguyen et al. for CO_2 adsorption in microporous carbon.[39,40] Point charges of the solid fluorinated graphene are obtained from our DFT calculations, as described below. The second term in the right-hand side of eq 2 is the Grimme's dispersion-corrected form of attractive interactions without the damping function of eq 1, since the repulsive term is explicitly included.[23] The repulsion coefficient C^{ij}_{12} is calculated following

$$\frac{C_{12}^{ij}}{C_6^{ij}} = \frac{(R_0^i + R_0^j)^6}{2} \quad (3)$$

Here, the parameters C_6 and R_0 are taken from Grimme's study on the long-range corrected semiempirical GGA-Type density functional.[26] The attractive and repulsive terms of the vdW energy obtained from eq 2 are equivalent to the corresponding terms in the usual 12−6 LJ representation

$$E_{\mathrm{LJ}}(r_{ij}) = 4\varepsilon_{ij}\left[\left(\frac{\sigma_{ij}}{r_{ij}}\right)^{12} - \left(\frac{\sigma_{ij}}{r_{ij}}\right)^{6}\right] \quad (4)$$

where ε_{ij} is the minimum-potential well depth, σ_{ij} is the distance, at which interatomic potential energy is zero and r_{ij} is the interparticle separation. In order to calculate ε and σ from eqs 2 and 4, the distances $(1/r_{ij})^{12}$ and $(1/r_{ij})^{6}$ for each cross-species were measured in an extended periodic cell of $3 \times 3 \times 3$ model (Figure 1) to account for vdW contributions of neighboring atoms, beyond which such contributions are negligible, as described by Zang et al.[24]

After an initial force field was generated using the DFT data described above, this force field was used to generate a new set of molecular configurations for water and CO_2 using GCMC. DFT-D2 energies of these newly generated configurations were then fitted to eq 4 once again to obtain a new set of interaction parameters (ε and σ). This procedure was repeated iteratively until the values obtained for ε and σ were converged,[23,25] which is achieved after three iterations here. In this way, a total of 905 and 676 molecular configurations were generated and fitted for water and CO_2, respectively. To ensure that our force field captures a broader range of possible energy states, DFT-D2 energies of all configurations, which were previously used for fitting in all iterations, were combined and again considered for fitting, from which the final LJ parameters (listed in Table S1) were calculated. We note that in this table the value of ε for the F−H pair is equal to zero, which arises from the fitting. This is consistent with the absence of LJ interactions for the hydrogen atom in SPC[38] and SPC/E[41] models of water. Figure 2 illustrates the agreement between our fitted potential and the full set of DFT-D2 interaction energies.

Modeling Fluorine-Doped CDC. We have developed atomistic models of fluorine-doped SiCDC at different levels of fluorination, having F/C atomic ratios of 0.019, 0.053 and 0.1, labeled as F-SiCDC.1, F-SiCDC.2 and F-SiCDC.3 respectively. The skeleton of all three models is based on a hybrid reverse Monte Carlo (HRMC) constructed model of SiCDC, recently developed in our laboratory,[18] that has shown good performance against a wide range of structural characterization, equilibrium and experimental kinetic uptake data for different gases.[18−21]

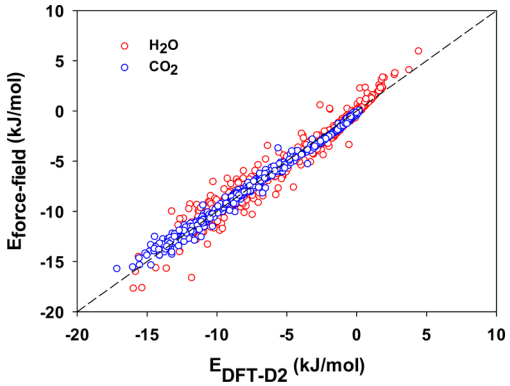

Figure 2. Comparison of the DFT-D2 energy with force field energy for H_2O and CO_2.

The virgin SiCDC model consists of 3052 carbon atoms in a 40 Å cubic unit cell. This model was subjected to fluorination of the carbon structure at the edges of carbon sheets, in addition to the carbon atoms with unsaturated bonding. Such unsaturated carbons are found in the amorphous SiCDC structure in substantial amounts, due to existence of various structural defects in this material.[18] The structure of the fluorinated models was then optimized using the conjugate gradient algorithm in GULP.[42,43] Bonded carbon−carbon interactions were modeled using the reactive EDIP force field.[44,45] Bonded F−C interactions consist of two-body and three-body interactions, for which the interaction parameters are given in Table S2. Nonbonded vdW interactions for F−F and F−C pairs applied during geometry optimization are calculated using the 12−6 LJ potential with cutoff distance of 10 Å. Details of LJ parameters used in this section are also provided in Table S2.

Partial charge distributions of the F-SiCDC models were determined based on the pattern derived from the charge distribution of the fluorinated graphene sheet, discussed above, in addition to the partial charge distribution of a sample fluorinated disordered carbon cluster removed from the original SiCDC model, as shown in Figure 3.

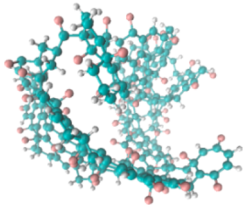

Figure 3. Fluorinated disordered cluster of carbon atoms removed from the virgin SiCDC model for charge calculations (nonfluorinated edge atoms saturated with hydrogen).

The reason for including charge distribution of the disordered cluster of carbon atoms in our investigation was to account for the effect of curvature on the distribution of partial charges in the charge pattern derived for the target F-SiCDC models. Details of calculations for DDEC charges obtained from the DFT-D2 energy of the disordered carbon cluster are similar to those discussed for the fluorinated graphene sheet in the previous section.

Our calculations showed that effects of structural curvature on distribution of partial charges are small. The charge distributions of the fluorinated graphene, as well as the disordered carbon cluster are presented in Table S3 and compared with the charge distribution pattern derived for the F-SiCDC models in this work. This table lists average partial charges of the first and second nearest carbon atoms, which are ultimately connected to one or two fluorine atoms in every given structure. For the F-SiCDC.1 model, having low level of fluorination, we have adopted a charge distribution analogous to that of the fluorinated graphene. However, for the other two models (F-

DOI: 10.1021/jacs.5b01105
J. Am. Chem. Soc. 2015, 137, 5969−5979

SiCDC.2 and F-SiCDC.3), where fluorine atoms have stronger effect on the second nearest neighboring carbons (i.e., second nearest carbons can be sometimes polarized by two fluorine atoms in their vicinity), the pattern derived in the current study for charge distribution has been utilized. Except for those atoms detailed in Table S3, other carbon atoms (i.e., carbon atoms beyond second nearest neighbor of fluorine) carry a constant partial charge of 0.004, 0.01, and 0.04 in F-SiCDC models 1 to 3, respectively, determined for electroneutrality of the unit cells. Snapshots of the virgin and fluorinated SiCDC models are illustrated in Figure 4.

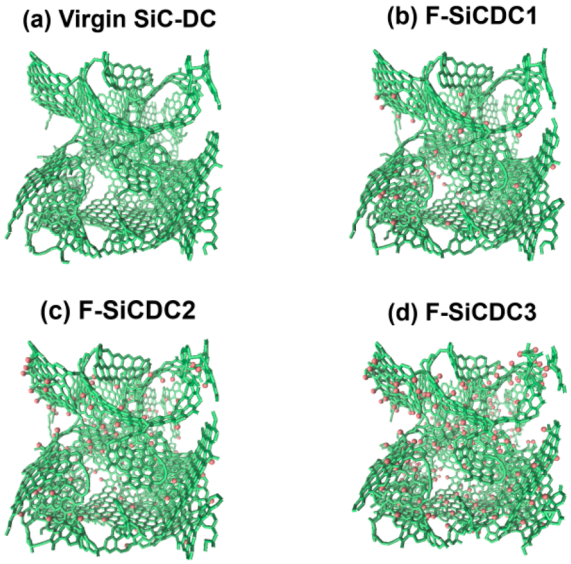

Figure 4. Virgin and fluorinated models of SiC-DC.

3. RESULTS AND DISCUSSION

Structural Characterization of Fluorinated SiCDC. Structural characterization of the models provides insight into simulated adsorption isotherms and transport properties of the system. Pore size distributions (PSDs) of the fluorinated models were determined using the spherical probe geometric approximation technique,[46,47] and are depicted in Figure 5. These distributions show a clear trend of pore volume reduction for pores in the range of 8−12 Å. More detailed information regarding structural properties of the models is provided in Table 1. The total pore volume (V_p), specific surface area (SA) and mean pore diameter of the SiCDC show slight decreases on fluorination, consistent with experimental results for fluorinated ACFs.[12−14]

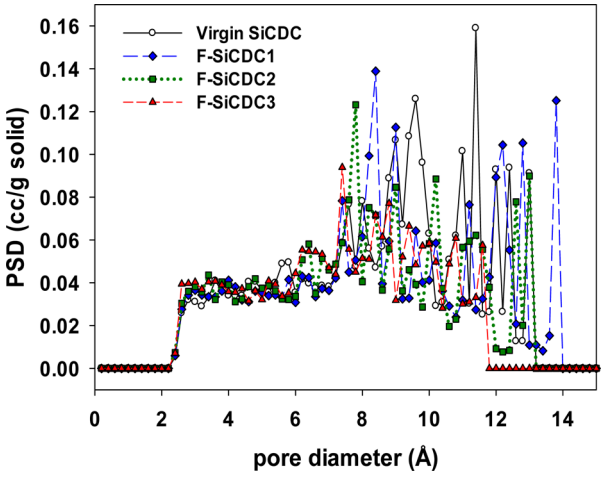

Figure 5. PSDs of the fluorinated models compared with that of virgin SiCDC.

The computational techniques for determination of accessible surface area and pore limiting diameter of the virgin and fluorinated models in our study are detailed elsewhere.[48] Here, pore limiting diameter is the diameter of the largest spherical probe that can permeate through the structure,[46,49] while the mean pore diameter is defined by 2 V_p^v/SA.

We note here the formation of large pores at ∼14 Å in F-SiCDC.1, and increase in mean pore diameter, despite reduction in pore volume (Table 1). This occurs on relaxation following structure optimization of the fluorinated carbon, and is a complex process that depends on the location of the randomly placed F atoms and the internal forces arising from the potential model. Clearly swelling of some parts of the structure along with shrinkage in others occurs. For example, it is seen that the peak at ∼9.5 Å in the virgin carbon is substantially lost in the fluorinated structures. This behavior is consistent with published experimental characterization data for fluorinated activated carbons, showing increased average micropore width despite apparent reduction of pore volume on fluorination.[14,16] Nevertheless, the 14 Å peak is however not seen here in the more highly fluorinated structures, F-SiCDC.2 and F-SiCDC.3, because their larger number of F atoms reduce the size of such larger pores, and lower pore volume.

Equilibrium Uptake of Water Vapor and CO_2 in F-SiCDC Models. We have investigated the equilibrium uptake of water vapor and CO_2 in all F-SiCDC models, and have compared the results with that for virgin SiCDC to demonstrate the effect of fluorination on adsorption of these gases. Adsorption isotherms of gases have been predicted by GCMC simulation, using the RASPA simulation package.[51] Water adsorption was predicted at 298 K and pressures up to saturation pressure of the SPC model[38] (3.26 kPa[52]). Subatmospheric adsorption of CO_2 was simulated at 273 K using the interaction model described by Nguyen et al.[39,40] In both cases, vdW interactions are computed using 12−6 LJ potential with cutoff distance of 34 Å in a simulation box containing a 2 × 2 × 2 array of unit cells. Electrostatic interactions are calculated using Ewald formalism with cutoff distance of 38 Å. Periodic boundary conditions are applied for all potential calculations. Several ab initio and empirical studies have demonstrated that curvature of graphene-like carbon sheets in nongraphitic carbon materials leads to enhanced atomic interactions between solid carbon and adsorbate molecules.[18,53−55] As suggested by these studies, we have applied a scaling factor of α = 1.1417 to all carbon (solid)-fluid cross-potential well-depths (ε_{c-f}) of the force field developed in this study, to account for the effect of carbon sheet curvature on the adsorption strength:

$$\varepsilon^{c-f}_{\text{Carbon}} = \alpha \varepsilon^{c-f}_{\text{Graphite}} \quad (5)$$

The scaling factor α is usually applied to modify the value of $\varepsilon^{c-f}_{\text{Graphite}}$, which is traditionally obtained using the Lorenz−Berthelot mixing rules with the C−C well-depth of 28 K, originally estimated by Steele for the interaction of adsorbate molecules with graphitized carbon black.[56] However, in this study, we have applied this scaling factor on carbon (solid)-fluid parameters of our own force field to account for the effect of

DOI: 10.1021/jacs.5b01105
J. Am. Chem. Soc. 2015, 137, 5969−5979

Table 1. Structural Properties of Fluorinated and Virgin Models

	fluorination level (F/C)	unit cell density (g/cm^3)	V_p^v (cc/g)^a	V_p^r (cc/g)^b	SA (m^2/g)^c	mean pore diameter (Å)^d	pore limiting diameter (Å)	maximum pore diameter (Å)
virgin SiCDC	0.00	0.951	0.674	0.564	1866	7.23	7.44	13.14
F-SiCDC.1	0.019	0.995	0.639	0.533	1755	7.28	7.72	13.98
F-SiCDC.2	0.053	1.044	0.573	0.487	1682	6.82	7.29	13.04
F-SiCDC.3	0.10	1.092	0.485	0.431	1554	6.24	6.99	11.6

^{a}Helium accessible pore volume using the second virial approach[50] $V_p^v = (1/(m_s)) \int e^{-\phi(r)/k_BT}\, dr$. ^{b}Pore volume using geometric approximation technique with hard sphere helium probe ^{c}Accessible surface area using hard sphere helium probe ^{d}Mean pore diameter = 2 V_p^v/SA

carbon sheet curvature in disordered SiCDC-based structures. The original and scaled parameters are both provided in Table S1.

As depicted in Figure 6, fluorination significantly enhances uptake of water, in apparent contrast with experimental observations of decreased water adsorption after fluorination,[14,15] so that the effect of pore volume and surface area reduction is completely overshadowed. As seen in this figure, higher levels of fluorination lead to higher water uptake. We note that the last data point in the water isotherm of F-SiCDC.2, as well as the last 6 data points in the water isotherm of F-SiCDC.3 (i.e., for $P/P_o > 0.7$) are not fully equilibrated, although they are close to equilibration, as shown in the Supporting Information (Figure S1–S3). The equilibration of water at high relative pressures in the fluorinated systems was extremely time-consuming. Nevertheless, this does not affect our finding regarding the increasing trend of water isotherms in the fluorinated systems, since full equilibration will achieve even higher adsorbed amounts. Consequently, we can conclude that fluorination increases hydrophilicity, evident also from the fully equilibrated low pressure data points reported in Figure 6. This is consistent with the experimental observation of enhanced water uptake below P/P_o of 0.5 by Parmentier et al.[16] In particular, it may be seen that for the most highly fluorinated SiCDC, model 3, $\partial^2 n/\partial P^2 < 0$ for $P/P_o < 0.4$ (Figure 6 inset), albeit weakly, a clear indication of hydrophilicity in this region. On the other hand the isotherms are fundamentally different from those of Li et al.,[14] suggesting that the covalent F–C bonding arising in their system is not pertinent to our fluorinated structure. Alternately, their isotherms may be different because they are affected by increased internal barriers for water diffusion (demonstrated later in this paper), while our GCMC-based isotherms are not affected by such barriers.

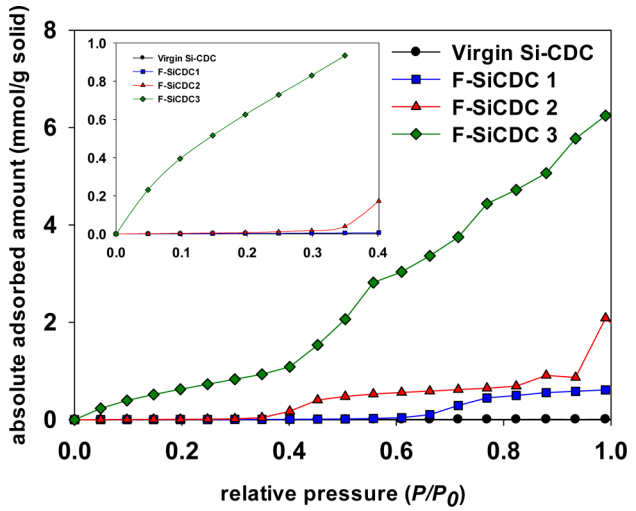

Figure 6. Predicted adsorption isotherm of water. Inset shows expanded view of low pressure region, $P/P_o < 0.4$.

Analysis of the isosteric heat of adsorption and the contributions of adsorbate–adsorbent and adsorbate–adsorbate interactions (Figure 7 (a–c)) clearly shows that water molecules are more strongly attracted to the pore walls in the fluorinated systems compared to the virgin material. As depicted in Figure 7 (c), F-SiCDC.2 model shows a steep

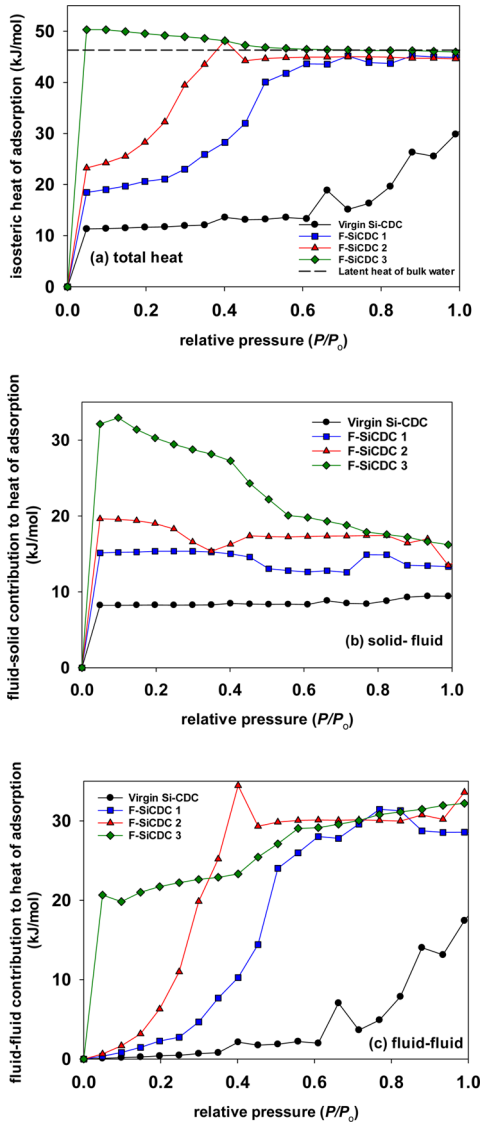

Figure 7. (a) Isosteric heat of adsorption of H_2O, and (b) fluid–solid and (c) fluid–fluid interaction contributions.

DOI: 10.1021/jacs.5b01105
J. Am. Chem. Soc. 2015, 137, 5969–5979

rise of fluid−fluid interactions at relative pressure of about 0.2, an indication of the initiation of pore filling. However, the F-SiCDC.1 model shows more gradual filling, with initiation of pore filling near relative pressure of 0.3. The slope in the fluid−fluid interaction increases with increase in pressure for the fluorinated systems indicating lower hydrophobicity of these systems compared to the virgin material. The F-SiCDC.3 model has a high fluid−fluid interaction energy (magnitude >20 kJ/mol) even at the lowest pressure sampled. This suggests very early initiation of filling of some part of the pore space at very low pressures not captured in this figure, an indication of much lower hydrophobicity. The dominance of the fluid−fluid contribution to the heat of adsorption shows that interadsorbate interactions are more significant at elevated pressures. This is not surprising since hydrogen bonding stabilizes formation of water clusters at pressures close to the saturation pressure of water.[57−62] In our previous studies on adsorption of water vapor in the hydrophobic virgin SiCDC, we showed that such clusters barely form below saturation pressure.[63] Nevertheless according to Figure 6, pore filling starts well below the saturation pressure for the fluorinated systems. A key question is then what provides the seed for early clustering of water molecules in the fluorinated systems?

To address this question, vdW and Coulombic contributions to fluid−fluid and solid−fluid interactions have been calculated at low pressure points, where hydrogen bonding is not significant. As illustrated in Figure 8, solid−fluid vdW interactions are the strongest interatomic interactions at these pressures, which also show an increasing trend with the level of fluorination of the models. In this figure, we have provided the results for the virgin SiCDC, as well as F-SiCDC.1 and F-SiCDC.2. The results from the F-SiCDC.3 model are not provided here as they require extremely lengthy simulations for convergence. Nevertheless, we do not expect to see any difference in the pattern, which is reported here for the other three porous carbons.

As seen here, solid−fluid vdW interactions seem to be the main governing interatomic potential at low pressures. The results above suggest that fluorination gives rise to enhancement of vdW interactions between water molecules and the pore walls. Comparison of the potential strengths of F−O and C−O pairs in Table S1 suggests that F−O interactions are more important in this regard than C−O pairs. The radial distribution functions of F−O pairs for different F-SiCDC models at the lowest pressure indicate apparent increase adsorbate multilayers (or water clustering), as seen in Figure 9 (a), considering the magnitude of the second RDF peak relative to the first is larger for the systems with higher fluorination.

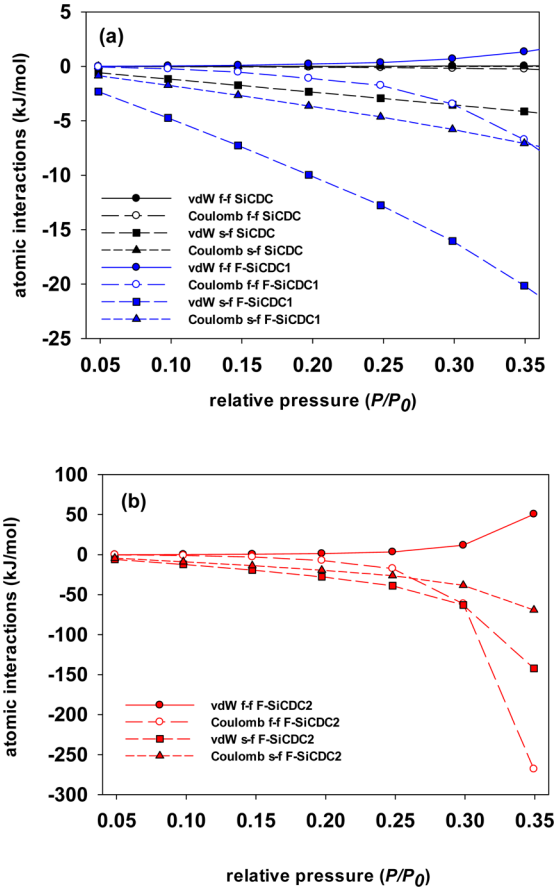

Figure 8. Fluid−fluid and solid−fluid contributions of vdW and Coulombic interactions of (a) virgin SiCDC and F-SiCDC.1 and (b) F-SiCDC.2, at low relative pressures.

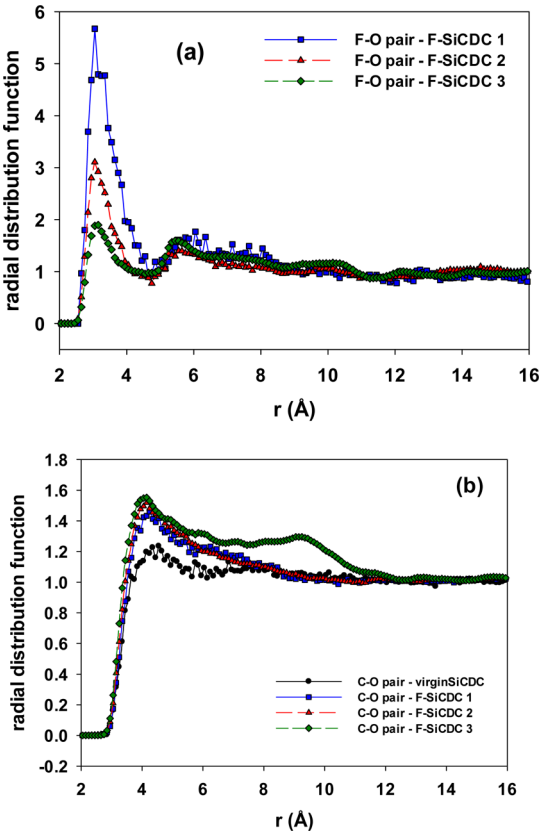

Figure 9. RDFs of the (a) F−O and (b) C−O pairs at the lowest pressure (P/P_o = 0.05).

The decrease in magnitude of the first RDF peak in Figure 9 (a) relates to the presence of water predominantly in the most highly confined (thus more energetic) pore regions, which are filled first at the low pressure, P/P_o = 0.05, at which the RDF is determined. On increasing fluorination the decreased hydrophobicity (or increased hydrophilicity) leads to a disproportionately larger amount of water going into the smallest pores (the most confined regions), which provide the most energetic spaces. This increases the water clustering, and reduces the

DOI: 10.1021/jacs.5b01105
J. Am. Chem. Soc. 2015, 137, 5969−5979

intensity of the first peak after averaging over all F−O pairs in the carbon.

In contrast, Figure 9 (b) shows that formation of such multilayer structures is weaker around carbon atoms in the virgin and F-SiCDC.1 as well as F-SiCDC.2 carbons, with the first peak increasing in magnitude relative to the second for F-SiCDC.1 and F-SiCDC.2. Given the abundance of carbon over fluorine, this is an indication of weaker hydrophobicity or improved hydrophilicity, supported by the slight shift of the peak position to smaller C−O distance. The higher relative magnitude of the second peak for F-SiCDC.3 is clearly due to water clustering over the first shell due to much larger amount adsorbed at the same relative pressure of 0.05, evident in Figure 6, and is the case for both the F−O and C−O RDFs. The snapshots in Figure S4 of the Supporting Information provide evidence of water clustering in the small pore regions of the F-SiCDC.3 model.

Overall, Figure 8 and Figure 9 together indicate that fluorination encourages formation of the adsorbed phase around fluorine atoms at very low pressure due to stronger F−O vdW interactions in narrow pore regions. In addition, the increasing trend of water adsorption with pressure (Figure 6) suggests that once sufficiently large number of water molecules is adsorbed around fluorine atoms at low pressures, water molecules start to progressively evolve into stable molecular clusters, which is expected to be fast growing due to the increased fluid−fluid interactions at elevated pressures (Figure 7 (c)). Subsequently, such water clusters grow until they fill the entire pore space, which is generally seen in the pore filling mechanism of microporous carbon materials.[63,64]

On the basis of the above argument, fluorinated surfaces of carbon appear to be less hydrophobic than the virgin material. The highly fluorinated model 3 could reasonably be described as being hydrophilic. Our finding is further supported by a recent DFT study with the same functional used in our calculation on adsorption of water in C_4F (a stable fluorocarbon derivative of graphene). The study reveals anomalous superhydrophilicity of the fluorinated graphene,[65] although we note that dispersion-correction is not applied in the DFT-GGA calculations in that study.

Figure 10 depicts subatmospheric adsorption isotherms of CO_2 at 273 K. As illustrated here, fluorination decreases adsorption of CO_2 considerably even at the lowest level of fluorination. This unusual behavior is explained by the reduction in strongly adsorbing sites, evident from the variation of heat of adsorption with pressure discussed below.

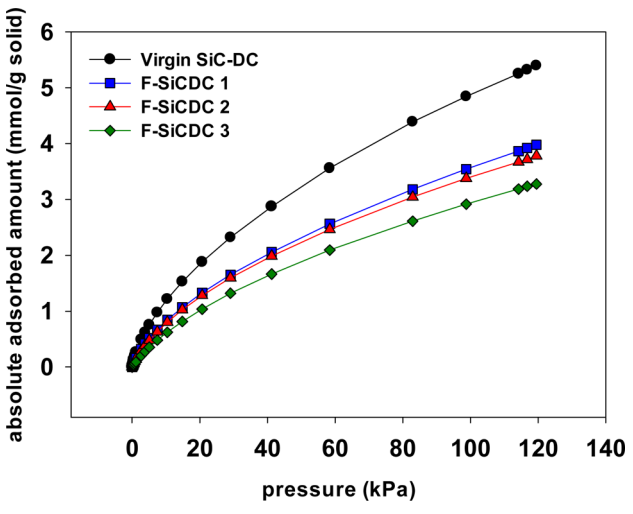

Figure 10. Subatmospheric adsorption isotherm of CO_2 at 273 K.

In Figure 11, it is seen that the steep drop in heat of adsorption of CO_2 at low pressure in the virgin SiCDC is absent in the fluorinated materials, indicative of elimination of the most strongly adsorbing sites on fluorination.

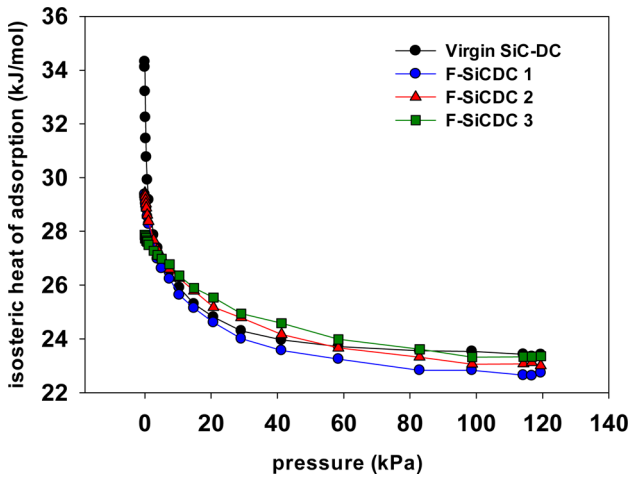

Figure 11. Isosteric heat of adsorption of CO_2.

This is supported by Figures S5 and S6 of the Supporting Information. Figure S5 shows steep drop in the solid−fluid contribution to the heat of adsorption at low pressure, on fluorination. Figure S6 demonstrates that fluorinated carbon has lower affinity toward CO_2 molecules compared to the virgin model, by virtue of significantly weaker vdW interactions. The reduction in the solid−fluid vdW interactions of the fluorinated model is mainly governed by the weaker C−O LJ interactions, which dominate the effect of other LJ interactions by virtue of its larger number. Thus, it is evident that the reduction in CO_2 adsorption arises from weakening of the solid−fluid interactions due to reduction in high energy sites on fluorination.

We have estimated the fractional density of states for H_2O and CO_2 in the virgin and F-SiCDC.1 models, based on the vdW energy of a single H_2O/CO_2 probe molecule at every grid point of a 50 × 50 × 50 grid network within the unit cell, and a Boltzmann occupancy factor. Figure 12 (a) shows that for H_2O there are more high energy states (E < −10.6 kJ/mol) in F-SiCDC.1 than in the virgin carbon, consistent with increased hydrophilicity. It also shows that there are fewer low energy states (E > −10.6 kJ/mol) for water in the fluorinated carbon compared to the virgin SiCDC. Interestingly, Figure 12 (b) shows that changes in distributions of high and low energy states are opposite for CO_2, supporting our argument that many of the high energy adsorption sites for CO_2 are lost in the fluorinated model compared to the virgin SiCDC.

Hydrophobicity of the Fluorinated Systems Due to Internal Energy Barriers. As discussed earlier, experimental measurements suggest that fluorination enhances hydrophobicity of microporous activated carbon. In contrast, our GCMC simulations predict a more hydrophilic mechanism for adsorption of water on fluorinated SiCDC. A plausible hypothesis to reconcile these observations is that fluorination leads to more strongly adsorbing sites for water, but this enhances internal free energy barriers within the structure and

DOI: 10.1021/jacs.5b01105
J. Am. Chem. Soc. 2015, 137, 5969−5979

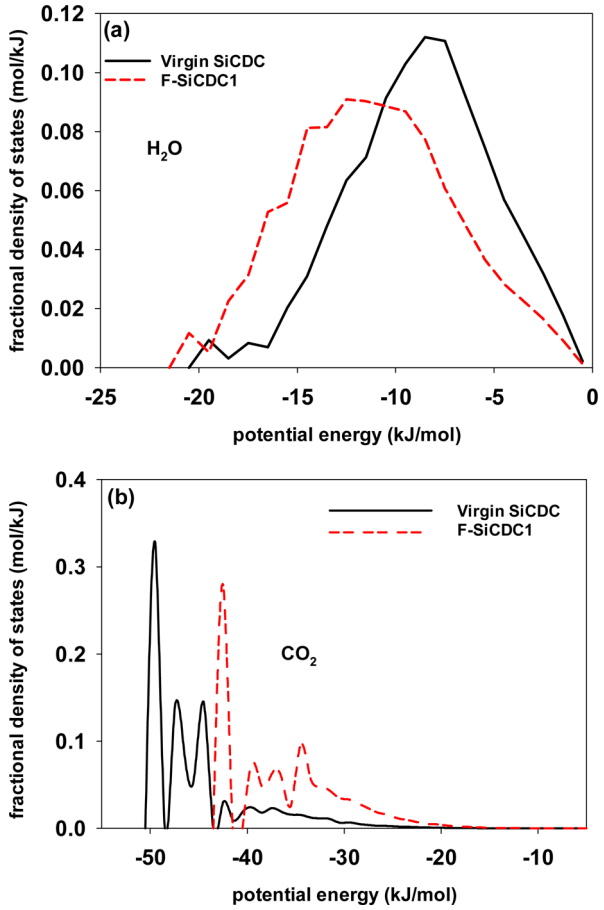

Figure 12. Fractional density of states in virgin and F-SiCDC.1 models for (a) water and (b) CO_2.

reduces pore accessibility. Since GCMC results are insensitive to such barriers, they will show increased equilibrium uptake of water on fluorination, while the experiment, which is sensitive to such barriers, can be negatively affected and not attain equilibrium on practical time scales.

To test this idea, we performed equilibrium molecular dynamics (EMD) simulation for both water and CO_2 in the fluorinated and virgin SiCDC models using LAMMPS.[66] The simulations were performed in the canonical (NVT) ensemble using a Verlet time integrator with a time step of 0.5 fs. Short-range intermolecular interactions were modeled using the 12−6 LJ potential with a cutoff distance of 18 Å in the 1 × 1 × 1 unit cell. Similar to the interaction parameters used for GCMC simulations, a scaling factor of 1.1417 was applied to all carbon (solid)-fluid cross-potential well-depths (ε_{c-f}) in the developed force field to account for the effect of carbon sheet curvature on the adsorption strength,[18,53−55] as detailed in Table S1. The standard Ewald formalism was employed for electrostatic interactions with cutoff distance of 18 Å, in such a way that pairwise interactions within this distance were computed directly and those outside this distance were calculated in reciprocal space. Periodic boundary conditions were applied on a rigid unit cell. Self-diffusivities for rigid models of water and CO_2 were calculated in the limit of infinite dilution (one molecule per unit cell) using the Einstein formulation for the mean squared displacement.[67] For every simulation 15 independent trajectories were collected to calculate mean-squared displacement (MSD) of the system after the molecules entered the Fickian region and traversed the entire lattice length. An example of converged MSD is illustrated in Figure S7 in the Supporting Information section. From the self-diffusion coefficients obtained at various temperatures, we have estimated the Arrhenius activation energy similar to our previous studies for diffusion of CO_2 and CH_4 in virgin SiCDC.[19]

Figure 13 demonstrates the temperature dependence of the self-diffusion coefficient of water and CO_2. Fluorine doping

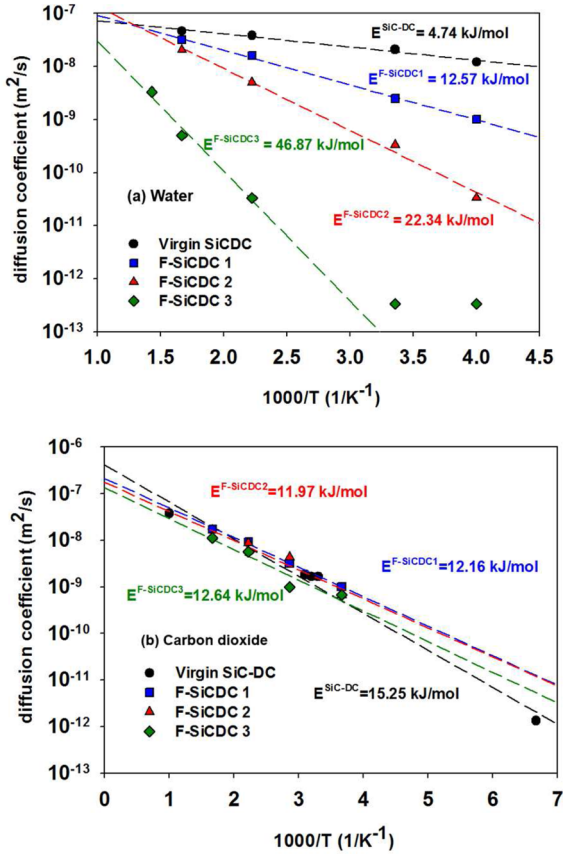

Figure 13. Variation of self-diffusion coefficient with temperature, for (a) water and (b) CO_2 in fluorine-doped and virgin SiC-DC models.

strongly increases the activation energy barrier (E_a) of the system for the diffusion of water. E_a for the F-SiCDC.3 model is almost 10 times larger than that of the virgin SiCDC. Correspondingly, there is a drop in the self-diffusion coefficient by about 5 orders of magnitude at 298 K. We found that the self-diffusion of water in the highly fluorinated system (i.e., F-SiCDC.3) is extremely slow at low and moderate temperatures (250−298 K), so that even after 200−400 ns of simulation time, water molecules have not entered the Fickian regime. The self-diffusivity of water at 250 and 298 K is of the order of 10^{-13} m^2/s, and for this low value of the diffusivity molecules are unable to traverse the entire unit cell for simulation times accessible using normally available computational resources. These two points are illustrated in Figure 13 (a) but not included in calculation of activation energy. Experimentally, energy barriers for transport of water in fluorinated SiCDC are likely to be even larger, because of the possibility of long-range barriers not captured by the present 40 Å unit cell. We have shown a similar scenario in our recent studies on adsorption of CO_2 in virgin SiCDC by comparing the simulation-based

DOI: 10.1021/jacs.5b01105
J. Am. Chem. Soc. 2015, 137, 5969−5979

diffusion coefficients with those obtained from kinetic uptake measurements, demonstrating simulation-based values to be several orders of magnitude larger.[68]

Indeed, the experimentally measured adsorption isotherm of water in pristine SiCDC sample is shown to have a very long equilibration time,[69] of the order of hours, indicating that adsorption of water is kinetically highly restricted in this material. Given the larger activation energy barriers of fluorinated models compared to the virgin SiCDC reported in this study, one predicts much smaller diffusion coefficients for fluorinated samples using the Arrhenius relation. On the basis of the change in activation energies, seen in Figure 13 (a), reduction in the diffusion coefficient by a factor of about 23.6, 1.2×10^3 and 2.4×10^7 respectively, is estimated for the three fluorinated carbons, since the change in pre-exponential factor will be much smaller. Thus, experimental observations in which hydrophobicity of the system is increased and adsorption of water is reduced in fluorinated activated carbons, can be reasonably explained by our results.[14,15]

In contrast to water, fluorination reduces the activation energy barriers for CO_2, as shown in Figure 13 (b). This finding is supported by a recent DFT study based on the use of GGA-PBE functional, in which Wu et al.[70] have shown that fluorine-modified porous graphene has a smaller energy barrier for CO_2 diffusion compared to the nonfluorinated graphene. In our study, the reduced CO_2 uptake (Figure 10), in addition to smaller solid–fluid heat of adsorption of this molecule (Figure S5 (a)), along with the decreased activation energy barriers of the fluorinated models for CO_2, suggest that fluorination reduces strength of the solid–fluid binding interactions for carbon dioxide.

To further support our finding regarding activation energy barriers of water and CO_2, we have investigated internal energy barriers of the systems for these molecules at infinite dilution based on analysis of the Helmholtz free energy map of the unit cell. In this method, initially developed by Haldoupis et al.[49] and subsequently extended by Sarkisov,[71,72] the difference between the minimum free energy of the unit cell along its percolation path, and the percolating free energy threshold of the unit cell along the same path, is defined as the limiting free energy barrier of the system. Figure 14 shows these energies for water and CO_2 at 298 K in the materials we considered.

As depicted here, the minimum free energy of the system is decreased with the level of fluorination for water, which is an indication of the enhanced hydrophilicity arising from fluorination of SiCDC. A similar conclusion can be made based on decreasing trend of the percolating free energy threshold for water. It is also evident from this figure that limiting free energy barrier of the system is significantly enhanced with increasing fluorination level. These results support our findings regarding the dual effect of fluorination, showing increasing hydrophilicity of the system, evident from GCMC simulation, together with increase in activation energy barriers for water obtained from EMD simulation.

In agreement with the results obtained from our GCMC and MD simulations, Figure 14 (b) suggests that fluorination weakens adsorption of CO_2 in F-SiCDC models and leads to reduction of the energy barrier of these systems for CO_2. In general, reduction of the activation energy barrier for CO_2, with simultaneous increase of the energy barrier for water vapor, suggests that fluorination can effectively improve selectivity of CO_2 over H_2O in CO_2/H_2O mixtures, at least in the limit of infinite dilution.

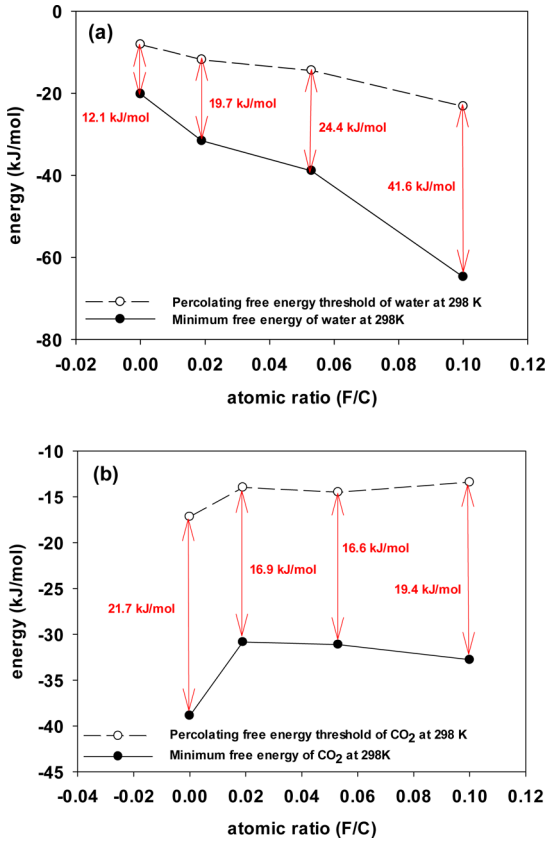

Figure 14. Limiting free energy barriers for (a) water and (b) CO_2 at 298 K, obtained from analysis of the free energy landscape of the system.

4. CONCLUSION

Our studies demonstrate that fluorination decreases the pore volume, surface area and mean pore diameter of SiCDC, in agreement with experiment. Comparison of the simulated adsorption isotherm of water in fluorinated SiCDC with that of the virgin material shows that fluorination considerably increases equilibrium uptake of water. On the other hand our computations, including calculation of activation energy barriers using MD simulations and analysis of the free energy map of the unit cells, demonstrate that fluorine doping remarkably increases internal energy barriers of the system for water vapor. These results explain the increase in hydrophobicity on fluorination of activated carbons, reported in the literature, as being an apparent effect that is governed by increase in internal energy barriers in the fluorinated system. The increase in internal energy barriers arises from stronger binding of fluid molecules inside the pore network, or decrease in hydrophobicity, as opposed to repulsion or steric hindrance to the diffusion of molecules through narrow pore entries. Thus, the results provide new insight into this apparently dual effect of fluorination, showing that while fluorination generates more hydrophilic carbon surfaces, they effectively act as more hydrophobic structures.

Further, we have demonstrated that fluorination gives rise to reduction of CO_2 uptake, despite decreasing internal energy barriers of the system for CO_2 diffusion. It is also shown that decrease of carbon dioxide adsorption is not due to physical restriction at pore entries but it is mainly because of the weakened solid–fluid binding energies after fluorination.

DOI: 10.1021/jacs.5b01105
J. Am. Chem. Soc. 2015, 137, 5969–5979

Finally, reduction of activation energy barriers for CO_2 on fluorination, as well as increase of these barriers for water vapor, suggests that this can improve selectivity of CO_2 over H_2O in CO_2/H_2O gas mixtures.

■ ASSOCIATED CONTENT

Supporting Information

Supporting tables and figures. The Supporting Information is available free of charge on the ACS Publications website at DOI: 10.1021/jacs.5b01105.

■ AUTHOR INFORMATION

Corresponding Author

*s.bhatia@uq.edu.au

Notes

The authors declare no competing financial interest.

■ ACKNOWLEDGMENTS

Helpful discussions with Dr. Hanjun Fang of Georgia Institute of Technology for development of the first-principles force field are gratefully acknowledged. We also thank Dr. George Opletal from RMIT University for providing an updated version of the PSD characterization tool. This research was supported by an Australian Research Council (ARC) Discovery grant. One of us (A.H.F.) acknowledges a Graduate School International Travel Award from The University of Queensland, to enable his collaborative visit to the Georgia Institute of Technology for a period of six months. D.S.S. was supported by UNCAGE-ME, an Energy Frontier Research Center funded by the U.S. Department of Energy, Office of Science, Basic Energy Sciences under Award #DE-SC0012577. This research was undertaken with the assistance of resources from the National Computational Infrastructure (NCI), which is supported by the Australian Government, through the National Computational Merit Allocation Scheme, as well as PACE (A Partnership for an Advanced Computing Environment) at the Georgia Institute of Technology, USA.

■ REFERENCES

(1) Ruff, O.; Bretschneider, O. *Z. Anorg. Allg. Chem.* **1934**, *217*, 1−18.
(2) Rüdorff, W.; Rüdorff, G. *Z. Anorg. Chem.* **1947**, *253*, 281−296.
(3) Wood, J. L.; Badachhape, R. B.; Lagow, R. J.; Margrave, J. L. *J. Phys. Chem.* **1969**, *73*, 3139−3142.
(4) Hamwi, A.; Alvergnat, H.; Bonnamy, S.; Béguin, F. *Carbon* **1997**, *35*, 723−728.
(5) Mickelson, E. T.; Huffman, C. B.; Rinzler, A. G.; Smalley, R. E.; Hauge, R. H.; Margrave, J. L. *Chem. Phys. Lett.* **1998**, *296*, 188−194.
(6) Norsten, T. B.; Guiver, M. D.; Murphy, J.; Astill, T.; Navessin, T.; Holdcroft, S.; Frankamp, B. L.; Rotello, V. M.; Ding, J. *Adv. Funct. Mater.* **2006**, *16*, 1814−1822.
(7) Park, S.; Lee, J.-W.; Popov, B. N. *Int. J. Hydrogen Energy* **2012**, *37*, 5850−5865.
(8) Hsieh, C.-T.; Chen, W.-Y.; Wu, F.-L. *Carbon* **2008**, *46*, 1218−1224.
(9) Hsieh, C.-T.; Chen, J.-M.; Huang, Y.-H.; Kuo, R.-R.; Li, C.-T.; Shih, H.-C.; Lin, T.-S.; Wu, C.-F. *J. Vac. Sci. Technol., B: Microelectron. Nanometer Struct.* **2006**, *24*, 113−117.
(10) Shen, B.; Chen, J.; Yan, X.; Xue, Q. *RSC Adv.* **2012**, *2*, 6761−6764.
(11) Yao, Z. Q.; Yang, P.; Huang, N.; Sun, H.; Wang, J. *Appl. Surf. Sci.* **2004**, *230*, 172−178.
(12) Setoyama, N.; Li, G.; Kaneko, K.; Okino, F.; Ishikawa, R.; Kanda, M.; Touhara, H. *Adsorption* **1996**, *2*, 293−297.
(13) Lee, Y. S.; Kim, Y. H.; Hong, J. S.; Suh, J. K.; Cho, G. J. *Catal. Today* **2007**, *120*, 420−425.
(14) Li, G.; Kaneko, K.; Ozeki, S.; Okino, F.; Touhara, H. *Langmuir* **1995**, *11*, 716−717.
(15) Li, G.; Kaneko, K.; Okino, F.; Touhara, H.; Ishikawa, R.; Kanda, M. *J. Colloid Interface Sci.* **1995**, *172*, 539−540.
(16) Parmentier, J.; Schlienger, S.; Dubois, M.; Disa, E.; Masin, F.; Centeno, T. A. *Carbon* **2012**, *50*, 5135−5147.
(17) Touhara, H.; Okino, F. *Carbon* **2000**, *38*, 241−267.
(18) Farmahini, A. H.; Opletal, G.; Bhatia, S. K. *J. Phys. Chem. C* **2013**, *117*, 14081−14094.
(19) Farmahini, A. H.; Shahtalebi, A.; Jobic, H.; Bhatia, S. K. *J. Phys. Chem. C* **2014**, *118*, 11784−11798.
(20) Farmahini, A. H.; Bhatia, S. K. *Carbon* **2015**, *83*, 53−70.
(21) Shahtalebi, A.; Farmahini, A. H.; Shukla, P.; Bhatia, S. K. *Carbon* **2014**, *77*, 560−576.
(22) Fang, H.; Demir, H.; Kamakoti, P.; Sholl, D. S. *J. Mater. Chem. A* **2014**, *2*, 274−291.
(23) Fang, H.; Kamakoti, P.; Zang, J.; Cundy, S.; Paur, C.; Ravikovitch, P. I.; Sholl, D. S. *J. Phys. Chem. C* **2012**, *116*, 10692−10701.
(24) Zang, J.; Nair, S.; Sholl, D. S. *J. Phys. Chem. C* **2013**, *117*, 7519−7525.
(25) Fang, H.; Kamakoti, P.; Ravikovitch, P. I.; Aronson, M.; Paur, C.; Sholl, D. S. *Phys. Chem. Chem. Phys.* **2013**, *15*, 12882−12894.
(26) Grimme, S. *J. Comput. Chem.* **2006**, *27*, 1787−1799.
(27) Kresse, G.; Hafner, J. *Phys. Rev. B: Condens. Matter Mater. Phys.* **1994**, *49*, 14251−14269.
(28) Kresse, G.; Furthmüller, J. *Phys. Rev. B: Condens. Matter Mater. Phys.* **1996**, *54*, 11169−11186.
(29) Blöchl, P. *Phys. Rev. B: Condens. Matter Mater. Phys.* **1994**, *50*, 17953−17979.
(30) Kresse, G.; Joubert, D. *Phys. Rev. B: Condens. Matter Mater. Phys.* **1999**, *59*, 1758−1775.
(31) Perdew, J. P.; Burke, K.; Ernzerhof, M. *Phys. Rev. Lett.* **1996**, *77*, 3865−3868.
(32) Manz, T. A.; Sholl, D. S. *J. Chem. Theory Comput.* **2010**, *6*, 2455−2468.
(33) Manz, T. A.; Sholl, D. S. *J. Chem. Theory Comput.* **2011**, *7*, 4146−4164.
(34) Watanabe, T.; Manz, T. A.; Sholl, D. S. *J. Phys. Chem. C* **2011**, *115*, 4824−4836.
(35) Manz, T. A.; Sholl, D. S. *J. Chem. Theory Comput.* **2012**, *8*, 2844−2867.
(36) Calero, S.; Dubbeldam, D.; Krishna, R.; Smit, B.; Vlugt, T. J. H.; Denayer, J. F. M.; Martens, J. A.; Maesen, T. L. M. *J. Am. Chem. Soc.* **2004**, *126*, 11377−11386.
(37) Wender, A.; Barreau, A.; Lefebvre, C.; Di Lella, A.; Boutin, A.; Ungerer, P.; Fuchs, A. H. *Adsorption* **2007**, *13*, 439−451.
(38) Berendsen, H. J. C.; Postma, J. P. M.; Van Gunsteren, W. F.; Hermans, J. In *Interaction Models for Water in Relation to Protein Hydration*, 14th Jerusalem symposium on quantum chemistry and biochemistry: "Intermolecular Forces", Jerusalem, 1981; Pullman, B., Ed.; Reidel: Dordrecht, 1981; pp 331−342.
(39) Hammonds, K. D.; McDonald, I. R.; Tildesley, D. J. *Mol. Phys.* **1993**, *78*, 173−189.
(40) Nguyen, T. X.; Bhatia, S. K.; Nicholson, D. *Langmuir* **2005**, *21*, 3187−3197.
(41) Berendsen, H. J. C.; Grigera, J. R.; Straatsma, T. P. *J. Phys. Chem.* **1987**, *91*, 6269−6271.
(42) Gale, J. D. *J. Chem. Soc., Faraday Trans.* **1997**, *93*, 629−637.
(43) Gale, J. D.; Rohl, A. L. *Mol. Simul.* **2003**, *29*, 291−341.
(44) Marks, N. A. *Phys. Rev. B: Condens. Matter Mater. Phys.* **2000**, *63*, 035401.
(45) Marks, N. A. *J. Phys.: Condens. Matter* **2002**, *14*, 2901.
(46) Gelb, L. D.; Gubbins, K. E. *Langmuir* **1998**, *14*, 2097−2111.
(47) Gelb, L. D.; Gubbins, K. E. *Langmuir* **1998**, *15*, 305−308.
(48) Sarkisov, L.; Harrison, A. *Mol. Simul.* **2011**, *37*, 1248−1257.

DOI: 10.1021/jacs.5b01105
J. Am. Chem. Soc. 2015, 137, 5969−5979

(49) Haldoupis, E.; Nair, S.; Sholl, D. S. *J. Am. Chem. Soc.* **2010**, *132*, 7528−7539.
(50) Talu, O.; Myers, A. L. *Colloids Surf., A* **2001**, *187*−*188*, 83−93.
(51) Dubbeldam, D.; Calero, S.; Ellis, D. E.; Snurr, R. Q. *Mol. Simul.* **2015**, 1−21.
(52) Liu, J. C.; Monson, P. A. *Langmuir* **2005**, *21*, 10219−10225.
(53) Klauda, J. B.; Jiang, J.; Sandler, S. I. *J. Phys. Chem. B* **2004**, *108*, 9842−9851.
(54) Nguyen, T. X.; Cohaut, N.; Bae, J.-S.; Bhatia, S. K. *Langmuir* **2008**, *24*, 7912−7922.
(55) Palmer, J. C.; Brennan, J. K.; Hurley, M. M.; Balboa, A.; Gubbins, K. E. *Carbon* **2009**, *47*, 2904−2913.
(56) Steele, W. A. *J. Phys. Chem.* **1978**, *82*, 817−821.
(57) Hummer, G.; Rasaiah, J. C.; Noworyta, J. P. *Nature* **2001**, *414*, 188−190.
(58) Kimura, T.; Kanoh, H.; Kanda, T.; Ohkubo, T.; Hattori, Y.; Higaonna, Y.; Denoyel, R.; Kaneko, K. *J. Phys. Chem. B* **2004**, *108*, 14043−14048.
(59) Brennan, J. K.; Bandosz, T. J.; Thomson, K. T.; Gubbins, K. E. *Colloids Surf., A* **2001**, *187*−*188*, 539−568.
(60) Müller, E. A.; Rull, L. F.; Vega, L. F.; Gubbins, K. E. *J. Phys. Chem.* **1996**, *100*, 1189−1196.
(61) Easton, E. B.; Machin, W. D. *J. Colloid Interface Sci.* **2000**, *231*, 204−206.
(62) Ohba, T.; Kanoh, H.; Kaneko, K. *J. Am. Chem. Soc.* **2004**, *126*, 1560−1562.
(63) Farmahini, A. H.; Bhatia, S. K. *Mol. Simul.* **2014**, *41*, 432−445.
(64) Nguyen, T. X.; Bhatia, S. K. *J. Phys. Chem. C* **2011**, 16606−16612.
(65) Wang, P.; Wang, H.; Yang, W. *Phys. Chem. Chem. Phys.* **2014**, *16*, 20464−20470.
(66) Plimpton, S. *J. Comput. Phys.* **1995**, *117*, 1−19.
(67) Gubbins, K. E.; Liu, Y.-C.; Moore, J. D.; Palmer, J. C. *Phys. Chem. Chem. Phys.* **2011**, *13*, 58−85.
(68) Shahtalebi, A.; Shukla, P.; Farmahini, A. H.; Bhatia, S. K. *Carbon* **2015**, *88*, 1−15.
(69) Bhatia, S. K.; Nguyen, T. X. *Ind. Eng. Chem. Res.* **2011**, *50*, 10380−10383.
(70) Wu, T.; Xue, Q.; Ling, C.; Shan, M.; Liu, Z.; Tao, Y.; Li, X. *J. Phys. Chem. C* **2014**, *118*, 7369−7376.
(71) Sarkisov, L. *Phys. Chem. Chem. Phys.* **2012**, *14*, 15438−15444.
(72) Sarkisov, L. *J. Phys. Chem. C* **2012**, *116*, 3025−3033.

DOI: 10.1021/jacs.5b01105
J. Am. Chem. Soc. 2015, 137, 5969−5979